

# A fixed-order time series model for damage detection and localization

Qipei Mei<sup>1</sup> · Mustafa Gül<sup>1</sup>

Received: 15 April 2016/Revised: 25 August 2016/Accepted: 28 September 2016/Published online: 7 October 2016  
© Springer-Verlag Berlin Heidelberg 2016

**Abstract** Time series modeling has great potential as a tool for damage detection. However, there are still a number of issues that need to be addressed before it can be effectively used for damage detection in the context of structural health monitoring (SHM). This paper presents a novel time series method directly derived from equation of motion (EOM) for damage detection. One of the unique advantages of the proposed method is that the order of the time series model is determined from the EOM, and thus, it is fixed, which could facilitate an easier automation and improve the computational efficiency. For the proposed method, fixed-order time series models are created for different sensor clusters using the output only vibration data from baseline and unknown states of the structure. Then, two different damage features (DFs) are developed from these models to identify the existence and location of the damage. To verify this method, an experimental steel grid structure with different damage cases applied is utilized. Two different DFs using fit ratios and coefficients are used to detect damage, and the results are compared. It is shown that the proposed method could identify the existence and location of damage and assess the relative severity successfully in most cases using either fit ratios or coefficients as DFs.

**Keywords** Structural health monitoring · Damage detection · Time series analysis · Sensor clustering

## 1 Introduction

Existing infrastructures are subjected to various potential risks, such as aging, fatigue, corrosion, overloading, and so on. These potential risks result in different levels of damage, which may cause the failure of members or even collapse of the entire structure. As infrastructure systems age and approach (or suppress) their design life, these problems become more significant. Taking bridges as an example, in the past, hundreds of bridges have failed due to all kinds of reasons. One of the critical reasons is poor maintenance, such as for Mianus River Bridge in the United States, Somerton Bridge in Australia, and CPR Bonnybrook Bridge in Canada [1–3]. Now, there are over 600,000 highway bridges in the US and more than 30 % of these bridges have exceeded their 50-year design life [4]. According to FHWA [5], nearly 10 % of these bridges are structurally deficient and 14 % are functionally obsolete. In Canada, condition of the infrastructures is also downgrading [6]. Mirza and Haider [7] indicated that nearly 80 % of existing bridges need repair to some extent. Recent years, many challenging bridges were successfully designed and constructed, but how to keep them safe and reliable with minimum costs during their lifecycle is still a big problem.

In this context, structural health monitoring (SHM) is considered as a valuable tool to increase safety and reliability, as well as to optimize maintenance operations during the service life of the infrastructure systems, offering considerable savings in life-cycle cost. SHM refers to a process of damage detection and condition assessment for aerospace, civil, and mechanical structures [8]. The importance of developing robust and automated SHM systems has been widely recognized in recent decades [9–15].

Damage detection is a very critical component of SHM given that the existence and location of damage should be

---

✉ Mustafa Gül  
mustafa.gul@ualberta.ca

<sup>1</sup> Department of Civil and Environmental Engineering,  
University of Alberta, Edmonton, AB T6G 2W2, Canada

identified, so that effective preventive actions could be taken [16]. Generally speaking, damage refers to the changes introduced into a system which lead to a decrease in its current and future performance. In structural systems, damage may be related to changes in the material and/or geometric properties, boundary conditions, and so on. According to Rytter [16], any damage detection method should focus on the following four objectives: (1) identifying the existence of damage; (2) localizing the damage; (3) determining the severity of damage; and (4) estimating the remaining useful life. These objectives belong to four different levels and are arranged in order of difficulty. Current damage detection methods mainly concentrate on levels 1, 2, and 3. Among all the objectives, the location of damage is paramount, because it is a prerequisite to conduct more detailed investigations and eventually understand the root cause of the damage.

Recent years, all kinds of methods based on different theories, such as modal frequencies, mode shapes or model updating, were developed by researchers [17–20]. Among all the methods, time series based methods [21–25] have drawn a lot of attention due to its advantages for computational efficiency and automation. Time series analyses are in general used to process time series data to extract the statistical characteristics of the data sets. Early in their development, these methods had been mainly used in economics and electrical engineering. In structural engineering, the time series model is initially used for system identification and modal analysis [26]. Gradually, the potential of time series analysis as a valuable tool for damage detection has been recognized by researchers. Dating back to 2000, Bodeux and Golinval [27] illustrated an autoregressive moving-average vector (ARMAV)-based method for system identification and damage detection on the “Steel-Quake” benchmark structure. The prediction error method was used to estimate the parameters of the ARMAV model on the basis of output data. The damage was identified based on the evaluation of the uncertainties of the parameters. However, as an early study, authors only attempted to identify the existence of the damage. In 2001, Sohn et al. [21] demonstrated an approach using time series analysis and outlier analysis. First, the time series analysis based on autoregressive models (AR models) and autoregressive models with exogenous inputs (ARX models) were carried out. Then, an outlier analysis based on Mahalanobis distance is conducted to extract the DF. Applying this method to the strain gage data of a surface-effect fast patrol boat, the method could distinguish different structural conditions. However, no information about location and severity was provided by this method. By applying the autoregressive moving-average (ARMA) model to the vibration signals, Nair et al. [22] proposed a new DF as a function of the first three AR coefficients. Then, a hypothesis test including the  $t$  test was used to detect damage. Furthermore, to discern the location of damage, two different

localization indices were introduced and the accuracies of results were compared. The results of applying the method to analytical and experimental data of the ASCE benchmark structure were encouraging, since the method was able to detect and locate damage correctly. Gül and Catbas [28] tested a statistical pattern recognition methodology in the context of time series analysis using different laboratory structures. The results showed that this methodology worked well in most cases. However, they also identified some issues that would have to be resolved before applying this approach in a realistic structure, such as the determination of the threshold. Gül and Catbas [29] introduced the concept of sensor cluster for the first time to improve the robustness of time series method for damage detection. In their study, coefficients and fit ratios of ARX models are used as DFs, respectively. Then, the DFs are verified first in a 4-DOF mass-spring system and then in an international benchmark problem. Their results demonstrated that the difference of fit ratio can identify the location and extent of damage successfully. Van Le and Nishio [30] conducted correlation coefficient analysis and outlier detection algorithm on the displacement and temperature data collected from a GPS monitoring system in a cable-stayed bridge. They then applied ARIMA model to those data to investigate the possibility of using such data for global damage detection. In 2014, Yao and Pakzad [31] created two DFs, i.e., the Mahalanobis distance of autoregressive coefficients and the Cosh distance of autoregressive spectra, to detect damage in a 10-DOF system. Analytical sensitivity analyses were conducted to derive the sensitivity of these DFs with respect to structural damage and measurement noise level. They showed that these DFs were more sensitive to damage than to noise. Roy et al. [32] developed a type of DF based on Kolmogorov–Smirnov test statistical distance and residual error of a set of ARX models. Evaluating the DFs in two numerical structures and an experimental structure, they observed that their DFs can satisfactorily localize damage in the presence of damping, multiple damages, and parametric uncertainties. Kim et al. [33] conducted a field experiment on a real Gerber-truss bridge to detect artificially induced damage. The authors first utilized Mahalanobis–Taguchi system (MTS) on modal parameters and then the indicators proposed by Nair et al. [22]. Their results showed that Nair’s indicator is superior to the modal parameters for damage detection.

As discussed above, the researchers in this area have conducted a lot of work and made great achievements. However, due to the complexity of civil infrastructure systems, environmental, and operational conditions, a number of issues still need to be resolved before they can be applied to real-life structures.

In most of the time series based methods, the order of time series models is often determined either by experience or by

the quality of models. The models would vary for different applications. In this paper, a fixed-order time series model is proposed for damage detection and localization. The sensor clustering approach for damage detection was introduced by Gül and Catbas [29], and the main novelty of this present paper is that the time series models are derived directly from the equation of motion (EOM) yielding to a fixed-order time series models. The model proposed by Gül and Catbas [29] did not explicitly consider the velocity and displacement data in the development of the time series models, whereas these parameters are included in the proposed models presented in this paper. These significant improvements in the model results in a consistent form of the time series models for any application and would be very beneficial for automation of the system. Based on the proposed models, two different DFs are developed and referred to as  $DF_{FR}$  and  $DF_{COEFF}$ , which stand for the DFs using fit ratio and coefficients. This is another main difference of the present paper with Gül and Catbas [29], where the damage features based on the model coefficients could not be used for damage detection, since they were too sensitive to measurement noise. It will be seen in the following sections that the proposed method could identify the location and severity of damage for a steel grid structure successfully using either fit ratios or coefficients as DFs.

## 2 Outline of damage detection method and underlying theory

### 2.1 Introduction to time series model

Time series modeling has been widely used in different fields including SHM. In this study, time series models are used to fit the dynamic response of a structure. In this section, a brief discussion about the autoregressive moving average model with eXogenous inputs (ARMAX model) and the autoregressive model with eXogenous inputs (ARX model) used in this paper is presented. More details of these time series models can be referred to Ljung [34] and Box et al. [35].

The basic form of an ARMAX model is shown in:

$$y(t) + a_1y(t - \Delta t) + \dots + a_{n_a}y(t - n_a\Delta t) = b_1u(t - \Delta t) + \dots + b_{n_b}u(t - n_b\Delta t) + e(t) + d_1e(t - \Delta t) + \dots + d_{n_c}e(t - n_c\Delta t), \quad (1)$$

where  $y(t)$ ,  $u(t)$ , and  $e(t)$  are output, input, and error terms of the model, respectively, and  $a_1, \dots, a_{n_a}, b_1, \dots, b_{n_b}, d_1, \dots, d_{n_c}$  are the parameters of the model. It is usually convenient to use the more concise form as in:

$$A(q)y(t) = B(q)u(t) + D(q)e(t), \quad (2)$$

where  $A(q)$ ,  $B(q)$ , and  $D(q)$  are the polynomials including coefficients of the model:

$$\begin{aligned} A(q) &= 1 + a_1q^{-1} + \dots + a_{n_a}q^{-n_a} \\ B(q) &= b_1q^{-1} + b_2q^{-2} \dots + b_{n_b}q^{-n_b} \\ D(q) &= 1 + d_1q^{-1} + d_2q^{-2} \dots + d_{n_c}q^{-n_c} \end{aligned} \quad (3)$$

where  $q$  is a backshift operator. For example, a variable  $X(t)$  at time  $t$  multiplied by  $q^j$  is equal to  $X(t-j\Delta t)$ . The orders of the polynomials are denoted by  $n_a$ ,  $n_b$ , and  $n_c$ .

Several other time series models are special cases of the ARMAX model. For example, the model is called an AR process if  $n_b$  and  $n_c$  are both zero, and an MA process if  $n_a$  and  $n_b$  are zero. If only  $n_c$  is set to zero, the model is defined as ARX model, which is used in the following sections. The form of an ARX model is expressed in Eq. 4 or Eq. 5. All the parameters have the same definitions as for ARMAX model:

$$y(t) + a_1y(t - \Delta t) + \dots + a_{n_a}y(t - n_a\Delta t) = b_1u(t - \Delta t) + \dots + b_{n_b}u(t - n_b\Delta t) + e(t) \quad (4)$$

$$A(q)y(t) = B(q)u(t) + e(t). \quad (5)$$

### 2.2 Least squares criterion

The first step to use an ARX model is to estimate its coefficients. In practice, least-squares criterion (LSC) is often used to estimate the coefficients of the ARX model. If data from previous time are used to represent the response at time  $t$ , the form in Eq. 6 could be obtained according to Eq. 4:

$$y(t) = -a_1y(t - \Delta t) - \dots - a_{n_a}y(t - n_a\Delta t) + b_1u(t - \Delta t) + \dots + b_{n_b}u(t - n_b\Delta t) + e(t). \quad (6)$$

The predicted value of  $y(t)$  could be calculated using:

$$\hat{y}(t) = -a_1y(t - \Delta t) - \dots - a_{n_a}y(t - n_a\Delta t) + b_1u(t - \Delta t) + \dots + b_{n_b}u(t - n_b\Delta t). \quad (7)$$

A more concise form of Eq. 7 is presented below:

$$\hat{y}(t) = \boldsymbol{\varphi}^T(\mathbf{t})\boldsymbol{\theta} \quad (8)$$

where

$$\boldsymbol{\varphi}(\mathbf{t}) = [-y(t - \Delta t) \quad \dots \quad -y(t - n_a\Delta t) \quad u(t - \Delta t) \quad \dots \quad u(t - n_b\Delta t)]^T \quad (9)$$

$$\boldsymbol{\theta} = [a_1 \quad a_2 \quad \dots \quad a_{n_a} \quad b_1 \quad \dots \quad b_{n_b}]^T \quad (10)$$

where  $\boldsymbol{\varphi}(\mathbf{t})$  is the regression vector consisting of known time series, and  $\boldsymbol{\theta}$  includes the coefficients to be estimated. Therefore, the error between true and predicted values of  $y(t)$  can easily be derived using the following:

$$e(t) = y(t) - \hat{y}(t) = y(t) - \boldsymbol{\varphi}^T(\mathbf{t})\boldsymbol{\theta}. \quad (11)$$

It can be seen that  $e(t)$  is actually the error term of the ARX model and it depends on the coefficients of the

model. Therefore, the least square criterion could be written in:

$$V_M(\theta) = \frac{1}{M} \sum_{t=1}^M \frac{1}{2} [y(t) - \boldsymbol{\varphi}^T(\mathbf{t})\boldsymbol{\theta}]^2, \tag{12}$$

where  $M$  stands for the number of points used in the model.

Since Eq. 12 is a quadratic criterion, analytic form of  $\theta$  to minimize  $V_M(\theta)$  could be derived, which is shown in Eq. 13:

$$\theta_M^{LS} = \arg \min V_M(\theta) = \left[ \frac{1}{M} \sum_{t=1}^M \boldsymbol{\varphi}(t)\boldsymbol{\varphi}^T(t) \right]^{-1} \left[ \frac{1}{M} \sum_{t=1}^M \boldsymbol{\varphi}(t)y(t) \right]. \tag{13}$$

There are also other search methods to determine a best model. Detailed derivations of other estimation methods can refer to Ljung [34].

### 2.3 ARX models based on different sensor clusters

The dynamic responses (accelerations, velocities, and displacements) of a structure are governed by the EOM. Changing over the time and strongly depending on prior states and external inputs, these data can be considered as typical time series. Therefore, it is expected that the time series modeling is suitable to fit these data and extract the statistical characteristics. However, different orders and coefficients would lead to different ARX models and the validity of models varies a lot according to different orders. The EOM of a structure under dynamic loading is investigated to determine proper orders of the ARX model. Equation 14 represents the basic form of an EOM for an  $N$  degrees of freedom (DOFs) system:

$$\mathbf{M}\ddot{\mathbf{x}}(\mathbf{t}) + \mathbf{C}\dot{\mathbf{x}}(\mathbf{t}) + \mathbf{K}\mathbf{x}(\mathbf{t}) = \mathbf{f}(\mathbf{t}) \tag{14}$$

The first step is to write the  $i$ th row of Eq. 15 separately (shown as Eq. 16):

$$\begin{bmatrix} m_{11} & \cdots & m_{1N} \\ \vdots & \ddots & \vdots \\ m_{N1} & \cdots & m_{NN} \end{bmatrix} \begin{Bmatrix} \ddot{x}_1 \\ \vdots \\ \ddot{x}_N \end{Bmatrix} + \begin{bmatrix} c_{11} & \cdots & c_{1N} \\ \vdots & \ddots & \vdots \\ c_{N1} & \cdots & c_{NN} \end{bmatrix} \begin{Bmatrix} \dot{x}_1 \\ \vdots \\ \dot{x}_N \end{Bmatrix} + \begin{bmatrix} k_{11} & \cdots & k_{1N} \\ \vdots & \ddots & \vdots \\ k_{N1} & \cdots & k_{NN} \end{bmatrix} \begin{Bmatrix} x_1 \\ \vdots \\ x_N \end{Bmatrix} = \begin{Bmatrix} f_1 \\ \vdots \\ f_N \end{Bmatrix} \tag{15}$$

$$(m_{i1}\ddot{x}_1(t) + \cdots + m_{iN}\ddot{x}_N(t)) + (c_{i1}\dot{x}_1(t) + \cdots + c_{iN}\dot{x}_N(t)) + (k_{i1}x_1(t) + \cdots + k_{iN}x_N(t)) = f_i(t) \tag{16}$$

$$(m_{i1}\ddot{\ddot{x}}_1(t) + \cdots + m_{iN}\ddot{\ddot{x}}_N(t)) + (c_{i1}\ddot{\ddot{x}}_1(t) + \cdots + c_{iN}\ddot{\ddot{x}}_N(t)) + (k_{i1}\ddot{x}_1(t) + \cdots + k_{iN}\ddot{x}_N(t)) = \ddot{f}_i(t). \tag{17}$$

Considering that measuring high-speed displacement and velocity data are usually not practical in most of the real life SHM applications, some efforts are made to eliminate these terms from Eq. 16. First, Eq. 17 is derived by taking the second derivative of Eq. 16. Then, the central difference technique is introduced to replace  $\ddot{\ddot{x}}_i(t)$  with  $(\ddot{x}_i(t + \Delta t) - \ddot{x}_i(t - \Delta t))/2\Delta t$  and  $\ddot{\ddot{x}}_i(t)$  with  $(\ddot{x}_i(t + \Delta t) - 2\ddot{x}_i(t) + \ddot{x}_i(t - \Delta t))/(\Delta t)^2$  [36]. Then, Eq. 18 is obtained with only accelerations. For free vibration, the force terms are zero, since the vibration is caused by initial conditions. Rearranging Eq. 18 and putting  $\ddot{x}_i(t + \Delta t)$  to the left of the equal sign as an output and all other terms to the right side as inputs, it is expected a form in Eq. 19 similar to the ARX model in Eq. 4:

$$\begin{aligned} & \left( m_{i1} \frac{(\ddot{x}_1(t + \Delta t) - 2\ddot{x}_1(t) + \ddot{x}_1(t - \Delta t))}{(\Delta t)^2} + \cdots + m_{iN} \frac{(\ddot{x}_N(t + \Delta t) - 2\ddot{x}_N(t) + \ddot{x}_N(t - \Delta t))}{(\Delta t)^2} \right) \\ & + \left( c_{i1} \frac{\ddot{x}_1(t + \Delta t) - \ddot{x}_1(t - \Delta t)}{2\Delta t} + \cdots + c_{iN} \frac{\ddot{x}_N(t + \Delta t) - \ddot{x}_N(t - \Delta t)}{2\Delta t} \right) \\ & + (k_{i1}\ddot{x}_1(t) + \cdots + k_{iN}\ddot{x}_N(t)) = \ddot{f}_i(t) \end{aligned} \tag{18}$$

where  $\mathbf{M}$ ,  $\mathbf{C}$ , and  $\mathbf{K}$  represent the  $N$  by  $N$  mass, damping and stiffness matrices of the system. The vectors  $\ddot{\mathbf{x}}(t)$ ,  $\dot{\mathbf{x}}(t)$  and  $\mathbf{x}(t)$  represent acceleration, velocity and displacement at a certain time  $t$ . The external forcing vector on the system is denoted by  $\mathbf{f}(t)$ .

If we write Eq. 14 in matrix form (see Eq. 15), it is seen that some transformations can be conducted on this EOM.

$$\begin{aligned} & \left( \frac{m_{ii}}{(\Delta t)^2} + \frac{c_{ii}}{2\Delta t} \right) \ddot{x}_i(t + \Delta t) = - \sum_{j=1:N, j \neq i} \left( \frac{m_{ij}}{(\Delta t)^2} + \frac{c_{ij}}{2\Delta t} \right) \ddot{x}_j(t + \Delta t) \\ & + \sum_{j=1:N} \left( \frac{2m_{ij}}{(\Delta t)^2} - k_{ij} \right) \ddot{x}_j(t) + \sum_{j=1:N} \left( \frac{c_{ij}}{2\Delta t} - \frac{m_{ij}}{(\Delta t)^2} \right) \ddot{x}_j(t - \Delta t). \end{aligned} \tag{19}$$

Comparing Eq. 19 with Eq. 4, the final form of the ARX model for the  $i$ th row of the Eq. 15 can be seen in the following equation:

$$\begin{aligned} \ddot{x}_i(t) = & b_{i1}^1 \ddot{x}_1(t) + \dots + b_{i,i-1}^1 \ddot{x}_{i-1}(t) + b_{i,i+1}^1 \ddot{x}_{i+1}(t) + \dots \\ & + b_{iN}^1 \ddot{x}_N(t) + b_{i1}^2 \ddot{x}_1(t - \Delta t) + \dots + b_{iN}^2 \ddot{x}_N(t - \Delta t) \\ & + b_{i1}^3 \ddot{x}_1(t - 2\Delta t) + \dots + b_{iN}^3 \ddot{x}_N(t - 2\Delta t) + e(t). \end{aligned} \quad (20)$$

Obviously, the ARX models for all the rows of Eq. 15 can be derived in the same way. When a structure is idealized as a multi-degree-of-freedom system, its stiffness and mass matrices are both sparse matrices and only the accelerations from some adjacent DOFs are adopted in each ARX model. Here, the sensor considered as output in the ARX model is defined as the reference channel and all the other sensors adjacent to this one are classified as the corresponding neighbor channels forming the sensor cluster. The orders of coefficients in ARX model are directly determined by comparing Eq. 19 with Eq. 20, and they would be fixed for any type of structures. Thus, for an  $N$ -DOF system,  $N$  different sensor clusters could be constructed.

To further clarify the proposed approach schematically, a simple 3-DOF mass spring system is taken as an example (shown in Fig. 1). For the first sensor cluster, the reference channel is the first DOF and the sensor cluster includes signals from DOFs 1 and 2. The second sensor cluster is created with the reference channel of DOF 2 and contains DOFs 1, 2, and 3 adjacent to the reference channel. Similarly, the third sensor cluster's reference channel is DOF 3 and the cluster comprises DOFs 2 and 3. For the total three DOFs, three sensor clusters are created and each ARX model corresponds to one sensor cluster.

### 2.4 Extraction of damage features

After creating the ARX models for the sensor clusters, two different DFs extracted from the ARX models are introduced to detect damage: (1)  $DF_{FR}$  and (2)  $DF_{COEFF}$ .  $DF_{FR}$  is defined as the difference of fit ratios. FR, i.e., fit ratio, is defined as normalized root mean squared error expressed as percentage, as presented in Eq. 21, in which  $y_{measured}$  is the measured output data,  $y_{model}$  is simulated output data,  $\bar{y}_{measured}$  is average of measured output data. As shown in Eq. 22,  $FR_1^i$  is obtained by fitting the damaged data to the  $i$ th ARX model based on baseline data, and  $FR_2^i$  is defined as the fit ratio obtained by fitting the damaged data to the  $i$ th ARX model based on damaged data. As the damage changes the properties of the structure, the ARX models based on baseline data cannot fit the damaged data as well as the ARX models based on damaged data. The difference

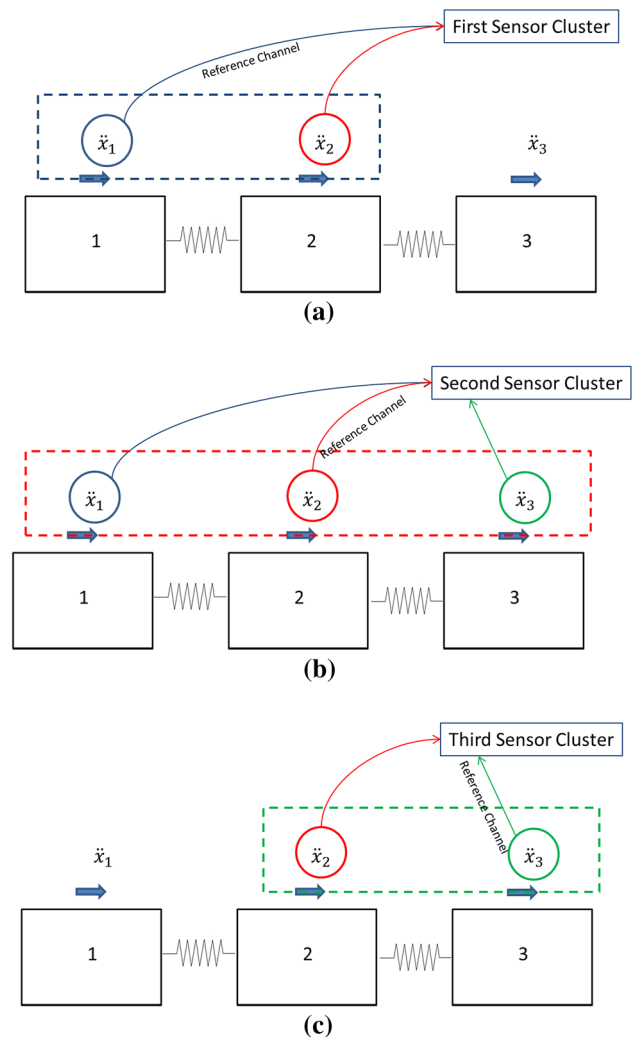


Fig. 1 Explanation of the sensor clustering schematically

between these fit ratios is expected to represent the change in the properties of the system when damage occurs:

$$DF_{FR}^i = 100 \left( 1 - \frac{\|y_{measured} - y_{model}\|}{\|y_{measured} - \bar{y}_{measured}\|} \right) \quad (21)$$

$$DF_{FR}^i = \frac{|FR_1^i - FR_2^i|}{FR_2^i}, \quad (i \in \text{sensor clusters}). \quad (22)$$

$DF_{COEFF}$  is based on the idea that if the ARX model can well fit the dynamic responses, the corresponding coefficients should reflect the physical properties of the structure as can be observed from Eq. 19. The damage caused by stiffness change is expected to be identified by calculating the square sum of the difference of the coefficients related to the stiffness.  $DF_{COEFF}$  is defined as:

$$DF_{COEFF}^i = \sum_{j=1}^N (b_{ij,H}^2 - b_{ij,D}^2)^2 \times 100, \quad (i \in \text{sensor clusters}), \quad (23)$$

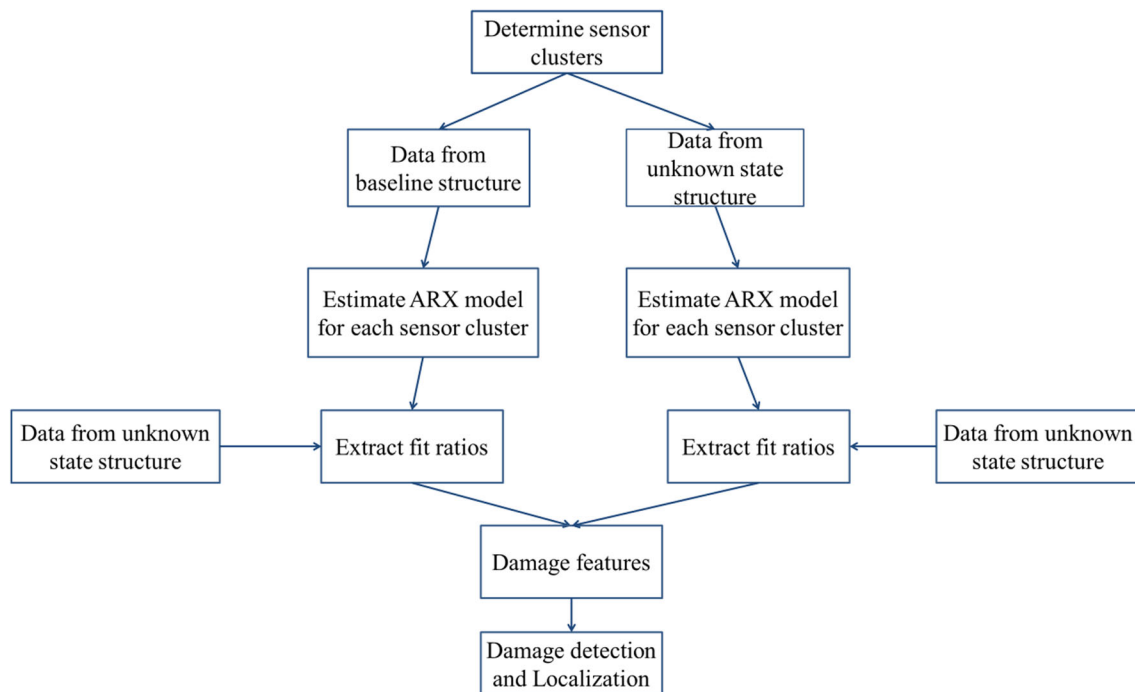


**Fig. 2** Process of the time series based method using  $DF_{FR}$

where  $b_{ij}^2$  stands for the coefficients for  $\ddot{x}_j(t - \Delta t)$  in the  $i$ th sensor cluster. The subscripts  $H$  and  $D$  represent the ARX models based on healthy and damaged data. The overall process for the method using two different DFs can be seen in Figs. 2 and 3.

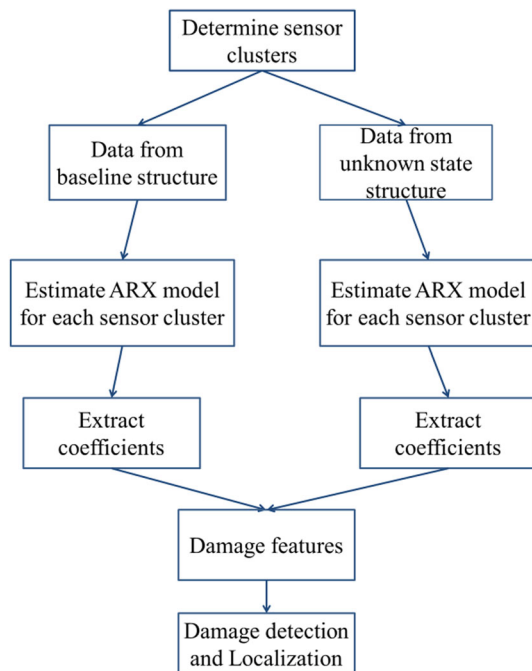


**Fig. 3** Process of the time series based method using  $DF_{COEFF}$

### 3 Experimental case study: a steel grid type structure

#### 3.1 Introduction to the benchmark problem and implementation of the method

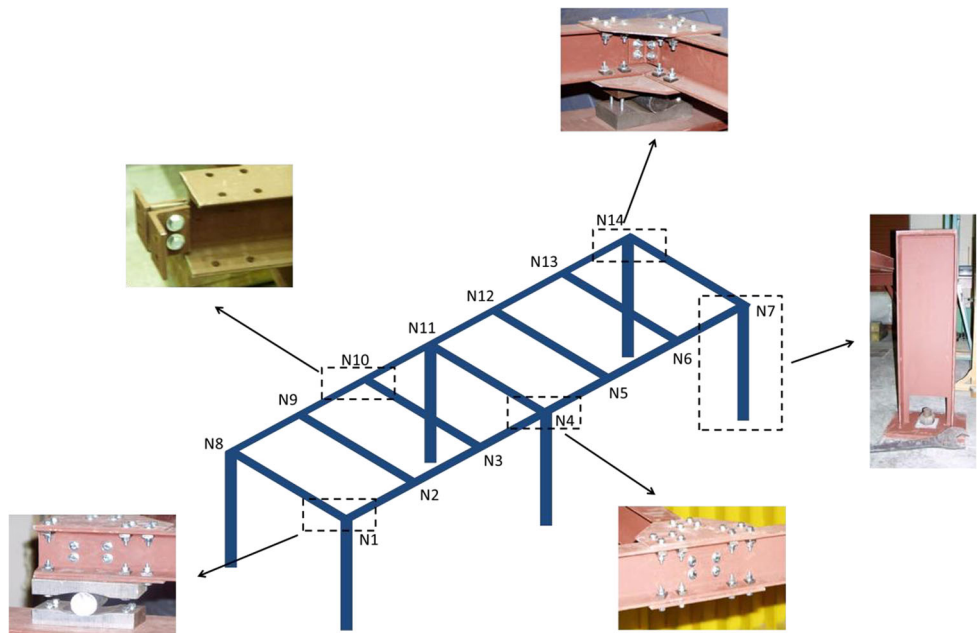
To investigate the capabilities of the proposed approach described in last section, it is applied to experimental data obtained from a bridge health monitoring benchmark problem developed and led by a research group at the University of Central Florida, USA [37]. The structure chosen as the benchmark problem is a steel grid, which enables researchers to test their methods before applying to real-life structures. As shown in Fig. 4, the specimen has two clear spans with two continuous girders across the middle supports. The girders are 5.49 m in longitudinal direction and the width of the structure is 0.92 m. The whole grid is supported by six 1.07 m tall columns. More details about the specimen can be found in Catbas et al. [37], and Gül and Catbas [29, 38].

As mentioned above, this grid structure is designed to be easily changeable to test the performance of various damage detection methods for different damaged states. In Fig. 5, the details of the grid structure can be seen. With the specially designed connections and supports, different boundary conditions (pin supports, roller supports, fixed supports, and semi-fixed supports) and damaged states (bolts removal, supports removal, and gusset plate removal) can easily be introduced.

**Fig. 4** Steel grid model used for experiments [23]



**Fig. 5** Details of the steel grid structure (adapted from [23])



The nodes which connect the girders and beams are numbered in Fig. 5. A number of sensors could be installed on this structure. For the purpose of dynamic tests, 12 accelerometers were installed in vertical direction at each node (except N7 and N14 for practical limitations during the tests). The accelerometers used in this study were IPC/seismic-type accelerometers. The parameters of the accelerometers were: 0.01–1200 Hz frequency range, 1000 mV/g sensitivity and  $\pm 2.5$  g measurement range. A VXI system from Agilent Technologies was used as the acquisition system to record the response. MTS-Test software was used for the purpose of acquisition control [23]. The sampling frequency for this experiment was 400 Hz.

For this study, four different kinds of damage were introduced. The detailed photos of the damage are shown in Fig. 6.

1. Damage Case 1: Scour (roller support removal) at N4.
2. Damage Case 2: Boundary restraint (fixing the roller supports) at N7 and N14.
3. Damage Case 3: Moment release (removal of all 24 bolts at the connection) and plate removal at N3.
4. Damage Case 4: Moment release (removal of 8 bolts connecting the transverse member to the main girder at each connection) at N3 and N10.

For the experiments, impact tests were conducted to simulate free vibration. The structure was excited by an

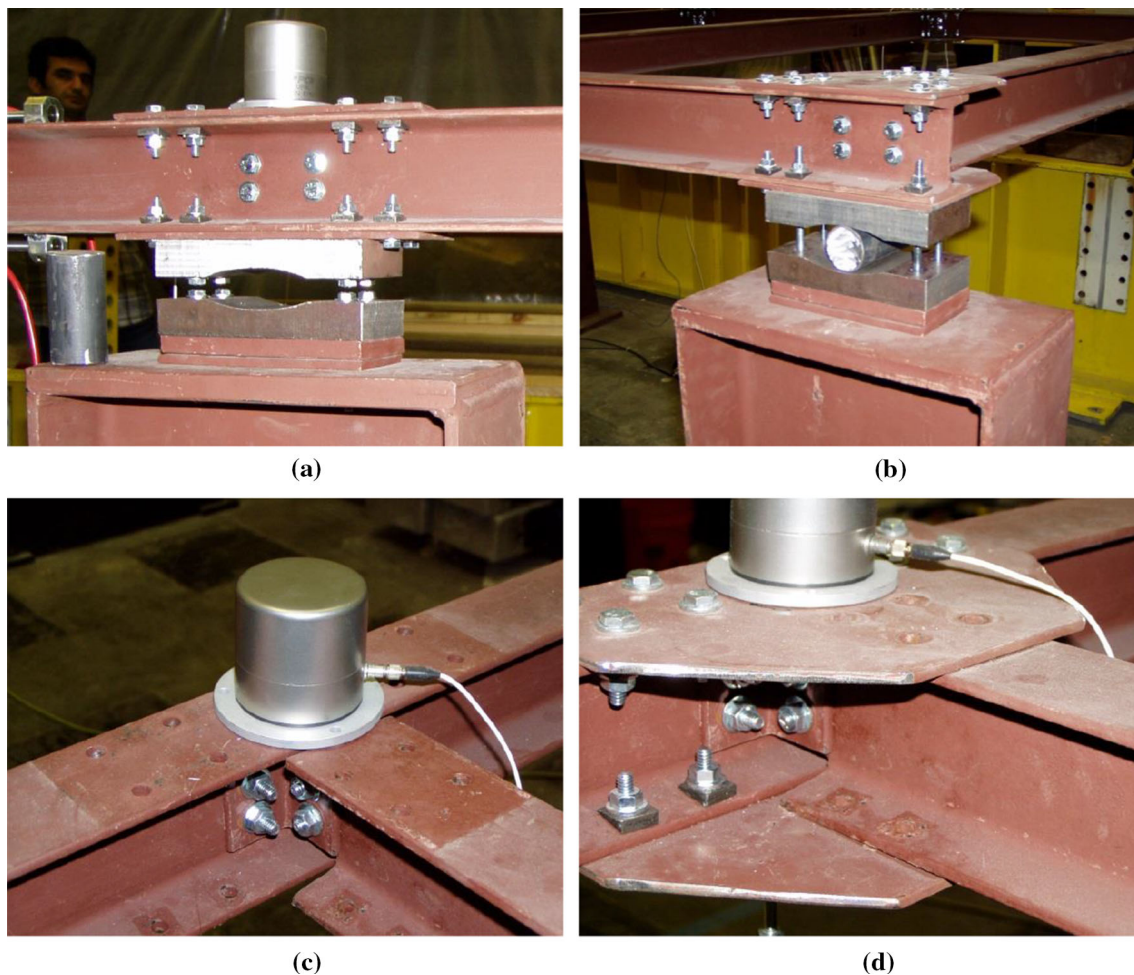


**Fig. 6** Detailed photos of damage simulations: **a** Damage Case 1; **b** Damage Case 2; **c** Damage Case 3; **d** Damage Case 4 [23]

instrumented impact hammer at N2, N5, N6, and N12 separately. For each damage case, 20 tests were carried out with five continuous ones at one excitation location. The sampling frequency, 400 Hz, is more than twice as the frequency for the 15th mode of the structure [23]. Thus, at least 15 modes could be identified in this structure, which is considered as a reasonable number for damage detection of bridge type structures. Figure 7 shows the experimental vibration data from the baseline (undamaged) structure at all 12 nodes. The total measured time period was 10 s, but only the data for the first 5 s were used for damage detection. To eliminate the effect of initial conditions, the first 100 data points (0.25 s) were not used.

For the implementation of the proposed damage detection method, the acceleration data from the support locations (N1, N4, N8, and N11) were practically zero and created instability in the models, since these sensors were on the supports. Eventually, as shown in Table 1, 8 sensors clusters with N2, N3, N5, N6, N9, N10, N12, and N13 as reference channels were formed to detect potential damage.

The following sections demonstrate the results and interpretations of the implementation of the proposed method with two different kinds of DFs. In Sect. 3.2, the difference of fit ratios is first considered as  $DF_{FR}$ . The results for impact at N12 are taken as an example (see Fig. 8) and for all other impact locations are used to investigate the influence of impact locations on the performance of the method. Section 3.3 presents the results obtained by using the function of coefficients as  $DF_{COEFF}$ . Only results for impact at N12 are shown for Sect. 3.3.

### 3.2 Analysis and result interpretations for the method using fit ratios as $DF_{FR}$

In general, a threshold value for the baseline condition should be determined to minimize the false negative and false positive alarms. For real-life applications, this threshold can be calculated using long-term data to eliminate the noise introduced by varying environmental and operational conditions and to separate damaged state from healthy state. In this study, the threshold is determined by

**Fig. 7** Experimental acceleration data for the baseline structure

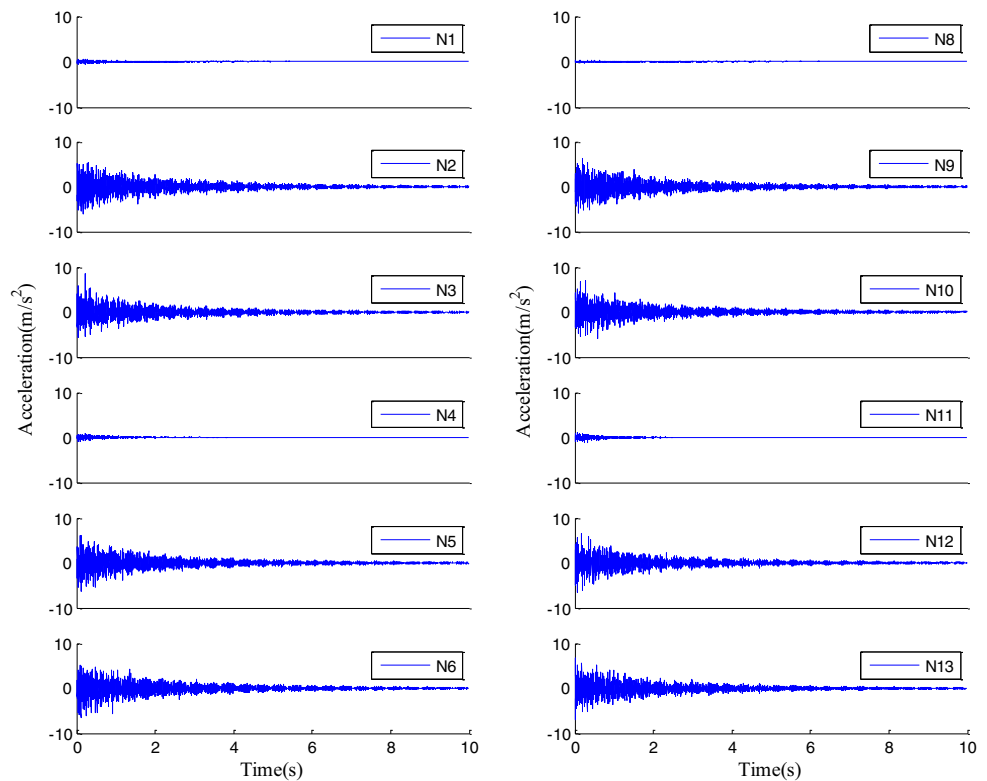


**Table 1** Sensor clusters for the steel grid structure

Sensor cluster	Output of the ARMAX model	Inputs of the ARMAX model
1	N2	N2, N3, N9
2	N3	N2, N3, N5, N10
3	N5	N3, N5, N6, N12
4	N6	N5, N6, N13
5	N9	N2, N9, N10
6	N10	N3, N9, N10, N12
7	N12	N5, N10, N12, N13
8	N13	N6, N12, N13

comparing two healthy states. Since the experimental tests used in this study are conducted in laboratory conditions, the threshold value is expected to be smaller compared to a real-life application.

Considering ten sets of healthy data as baseline state and the other ten sets as unknown states, the  $DF_{FR}$  can be obtained by applying the proposed damage detection method. Figure 9 shows all the  $DF_{FR}$  for the healthy case. It is easy to observe that almost all the  $DFs$  are below 0.9, so here the threshold is determined as 0.9 with 79 out of the 80 points below it. Note that a more rigorous statistical analysis or machine learning approach should be conducted for determining the threshold for real-life applications [39–41].

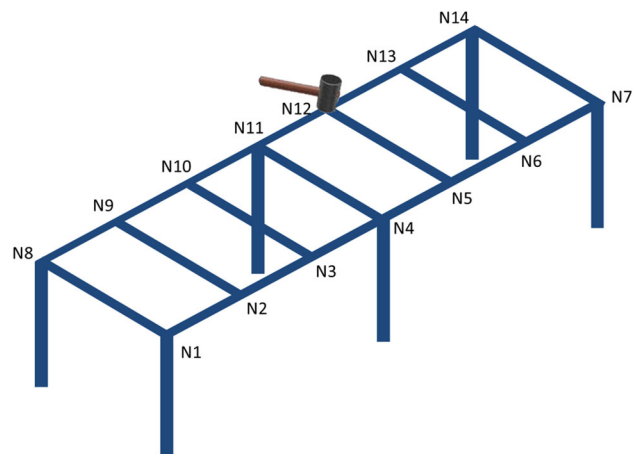


**Fig. 8** Location of the excitation

3.2.1 Damage detection using  $DF_{FR}$  for Damage Case 1 (DC1): scour (support removal) at N4

The  $DF_{FR}$  for Damage Case 1 are shown in Fig. 10. Since this is significant global damage, all the  $DF_{FR}$  are above the threshold. Although this global damage has influence on all the nodes in the structure, the proposed method still locates the damage through the values of  $DF_{FR}$ . It is shown in Fig. 10 that the  $DF_{FR}$  for N3 and N5 (actually they are very close due to the symmetry) are significantly larger than other nodes due to direct effect of the removal of roller

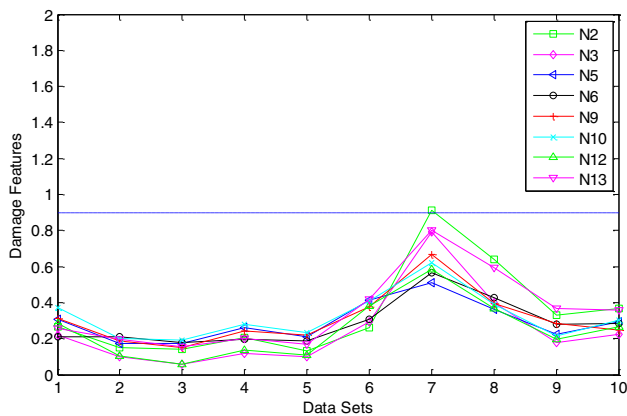


**Fig. 9**  $DF_{FR}$  for determining the threshold under free vibration

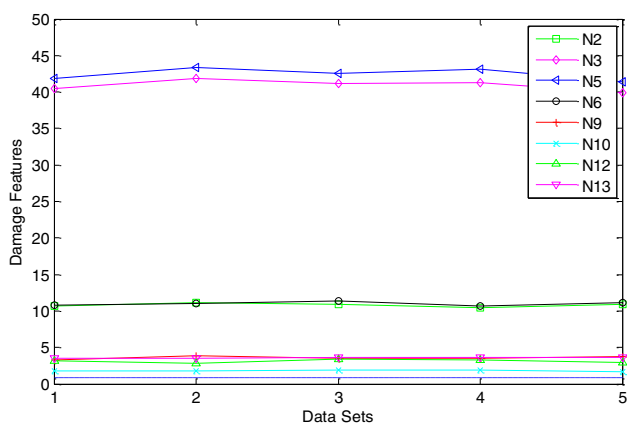


**Fig. 10**  $DF_{FR}$  for DC1 of the steel grid structure

support at N4. Interestingly, the acceleration data for N4 are not even used in any sensor clusters, but the damage is still reflected by the  $DF_{FR}$  from the neighboring sensors. In addition, the indirect effects of the damage on N2 and N6 also lead to high  $DF_{FR}$  at these nodes. Note that the  $DF_{FR}$  are around 40 for N3 and N5.

### 3.2.2 Damage detection using $DF_{FR}$ for Damage Case 2 (DC2): boundary restraint (fixing the roller supports) at N7 and N14

Damage Case 2 is a less severe case than the previous damage case, but it is still a relatively significant global damage case. All the  $DF_{FR}$  for this case (Fig. 11) are above the threshold also, because it is global damage affecting the entire structure significantly. Due to the boundary condition change at supports N7 and N14, the  $DF_{FR}$  for the closest nodes N6 and N13 are higher than  $DF_{FR}$  for all other nodes (note that N7 and N14 were not instrumented). Due to the influence of damage, the nodes N5 and N12 are also higher than others (but lower than N6 and N13,

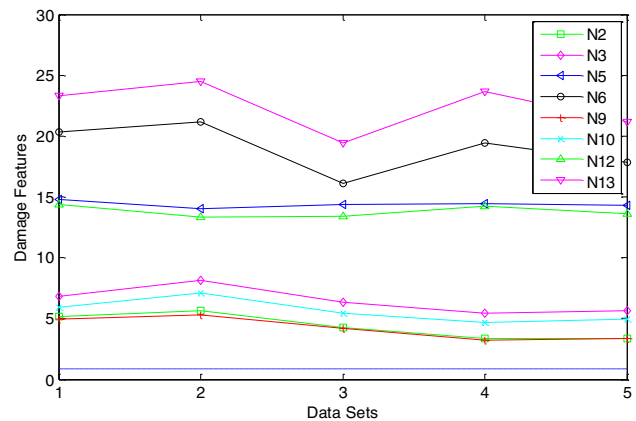


**Fig. 11**  $DF_{FR}$  for DC2 of the steel grid structure

because they are farther from damage). These results demonstrate that the method has ability to reflect the location of damage using the values of  $DF_{FR}$ . Note that the  $DF_{FR}$  for N13 are around 24 and for N6 are about 20. These values are smaller than those in Damage Case 1 showing that less severe damage occurs. The slight differences for  $DF_{FR}$  in N6 and N13 for different trials may be caused by some experimental variations.

### 3.2.3 Damage detection using $DF_{FR}$ for Damage Case 3 (DC3): moment release (removal of bolts) and plate removal at N3

Damage Case 3 is localized damage due to the removal of plate and bolts at N3. Figure 12 shows the  $DF_{FR}$  for each node. In this figure, only  $DF_{FR}$  for N2, N3, N9, and N10 are above the threshold, in which the  $DF_{FR}$  for N3 are the largest. All these evidences point out the correct location of the damage at N3. Moreover, due to the localized damage, other  $DF_{FR}$  are below the threshold. Also note that the maximum  $DF_{FR}$  in Damage Case 1 were around 40 and around 24 in Damage Case 2, but in this case, the maximum  $DF_{FR}$  is only about 6. This can be explained as that much less severe damage has happened in Damage Case 3. This is the case since such damage caused by removing bolts and a plate is localized and has less influence than the change of boundary conditions.

### 3.2.4 Damage detection using $DF_{FR}$ for Damage Case 4 (DC4): moment release (removal of bolts) at N3 and N10

Damage Case 4 introduces relatively minor damage by removing bolts at N3 and N10, and the  $DF_{FR}$  for all 8 sensor clusters are shown in Fig. 13. Obviously, the removal of bolts at one node is a localized damage, but the combination of such damage at two nodes is expected to

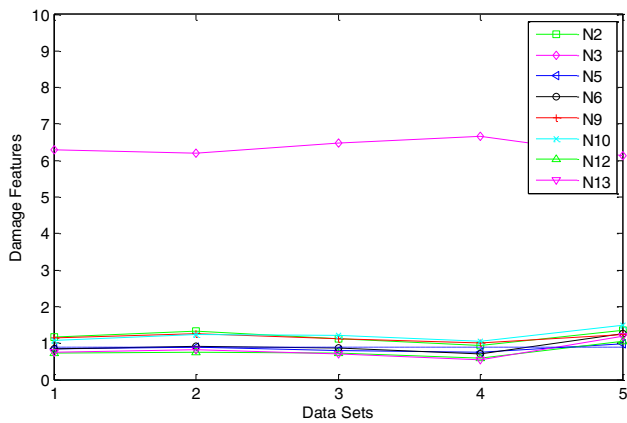


Fig. 12  $DF_{FR}$  for DC3 of the steel grid structure

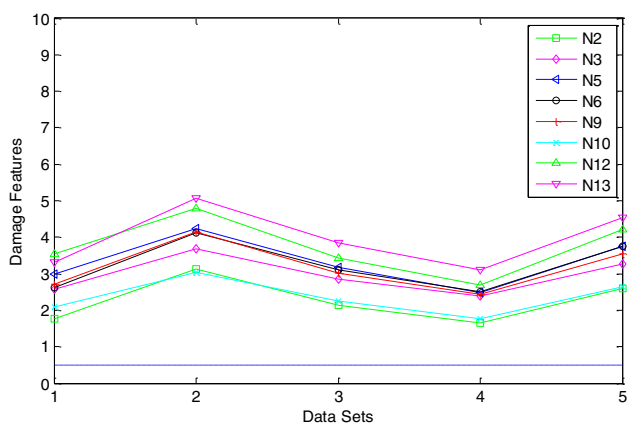


Fig. 13  $DF_{FR}$  for DC4 of the steel grid structure

have a more spread influence (actually, six out of eight sensors are adjacent to the damage in terms of sensor clusters). This can be the reason of why all the  $DF_{FR}$  are above the threshold, which shows the existence of damage. In this case, the highest  $DF_{FR}$  is about 5, the smallest in all four damage cases, which shows the severity of the damage. However, it is acknowledged that the levels of the  $DF_{FR}$  are higher than expected and the location of damage is not well identified, but all these  $DF_{FR}$  are very close and do not show false-positive results. The main reason to this failure can be the fact that the minor damage may have affected its adjacent nodes very similarly, which is difficult to distinguish.

### 3.2.5 Influence of the impact location on damage detection using $DF_{FR}$

In the last sections, the results obtained using the data with N12 as the impact location demonstrate that the method successfully identify, localize, and estimate the severity of the damage. However, in practice, different impact locations

would lead to different vibration and dynamic response from the same structure. To investigate the influence of impact location on the damage detection results using the time series based method, dynamic responses obtained by exciting the structure at N2, N5, and N6 are used in this section (shown in Fig. 14).

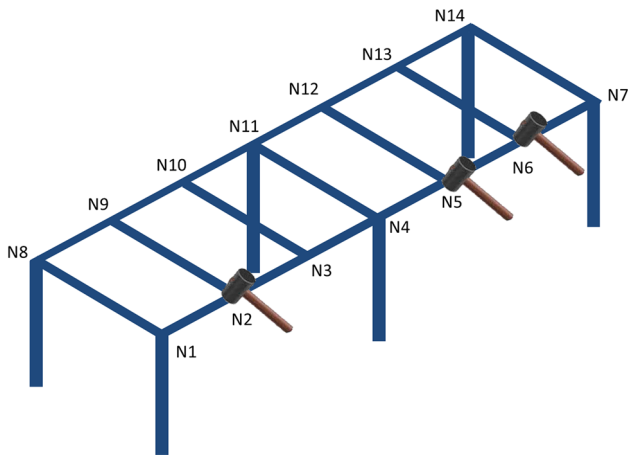
Figures 15, 16, 17, and 18 show the  $DF_{FR}$  adopting data from different impact locations. In these figures, data sets 1–5 stand for the results for excitation at N2, data sets 6–10 represent the results for excitation at N5, and data sets 11–15 demonstrate the results for excitation at N6. Note that the results for excitation at N12 were already presented in the previous section.

As shown in Fig. 15, the results for support removal at N4 in Damage Case 1 are presented. The  $DF_{FR}$  for N3 and N5 are still the highest as presented before. The indirect effects of the damage on N2 and N6 for all three excitation locations are obvious. Although the relationship of  $DF_{FR}$  between nodes is clear, the significance of difference still varies according to difference impact locations. For data sets 6–10 (impact location at N5), the values of  $DF_{FR}$  are lower than other sets, but the highest  $DF_{FR}$  of about 45 is still larger than the corresponding DFs for impact location 5 in Damage Case 2 (approximately 35). The difference of  $DF_{FR}$  is mainly caused by the reason that the impacts at different locations excite different modes, so that the goodness of fit of the ARX models would change accordingly; however, this does not affect the overall relationship of  $DF_{FR}$  between sensor clusters.

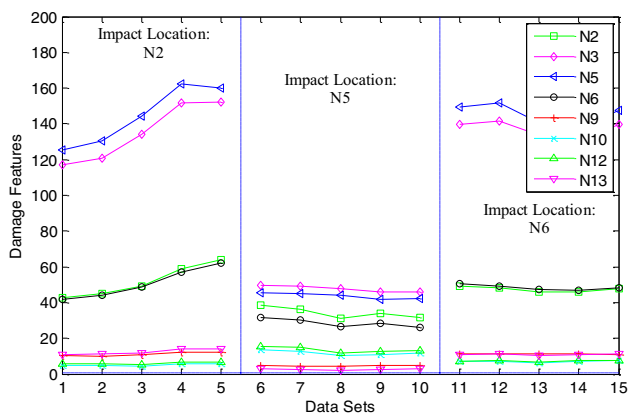
Figure 16 shows the  $DF_{FR}$  obtained by applying the method to Damage Case 2. In this figure, it can be seen that the method shows the  $DF_{FR}$  for N6 and N13 as the highest for all three impact locations despite some difference in the levels. Similarly, N5 and N12 are also standing out due to the indirect effect of the damage. All the other  $DF_{FR}$  are relatively low. Note that for data sets 1–10, the  $DF_{FR}$  for N3 and N10 are higher than for N2 and N9, but the case is inversed for data sets 11–15. This means that the impact location may slightly affect the relationship between  $DF_{FR}$  for the nodes far from the damage.

Figure 17 shows the results for Damage Case 3, which is plate and bolts removal at N3. For all three impact locations,  $DF_{FR}$  for N3 stand out exposing the correct location of damage. It is also seen that all other  $DF_{FR}$  are relatively low, but their relations to the threshold are undetermined. When the excitation is at N2, half of the  $DF_{FR}$  for other nodes are above the threshold, but this is not very obvious to the results for excitation at N5 and N6. This problem can be solved by determining the threshold separately for different impact locations.

In Fig. 18, the results for Damage Case 4 (bolts removal at N3 and N10) are shown. For three different excitation locations, all the  $DF_{FR}$  are all above the threshold, which is consistent with the results for impact at N12. However, the



**Fig. 14** Excitations at N2, N5, and N6



**Fig. 15**  $DF_{FR}$  for DC1 using dynamic responses excited at N2, N5, and N6

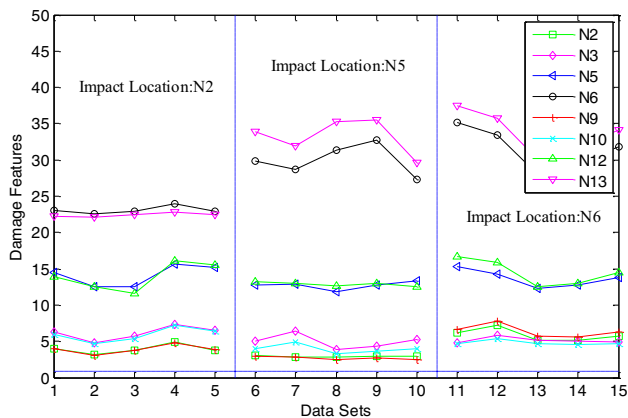


**Fig. 16**  $DF_{FR}$  for DC2 using dynamic responses excited at N2, N5, and N6

location of damage is still not detected for these three impact locations. This means that the results cannot be improved by choosing a more proper impact location.

Overall, it is shown that the location of the impact has only slight influence on the  $DF_{FR}$  for the nodes closest to the

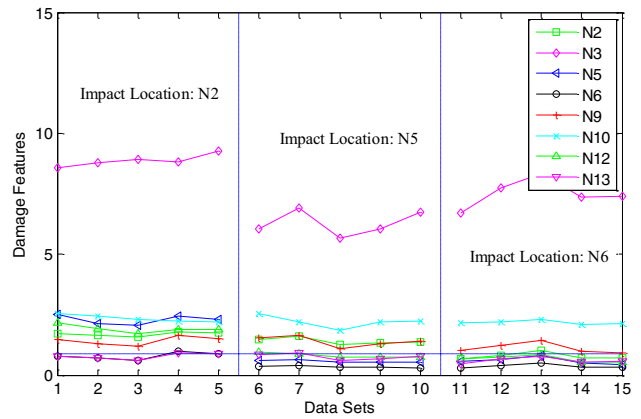


**Fig. 17**  $DF_{FR}$  for DC3 using dynamic responses excited at N2, N5, and N6

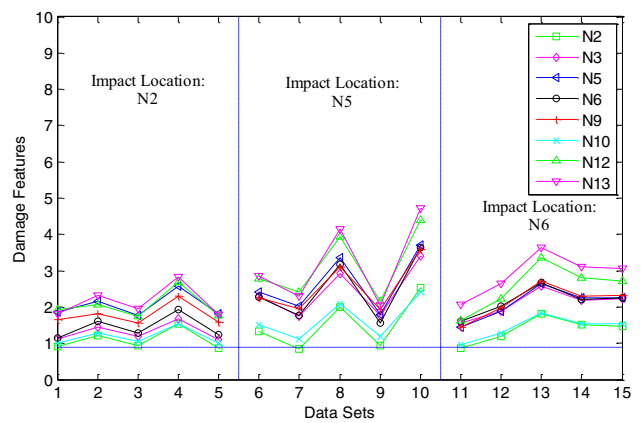


**Fig. 18**  $DF_{FR}$  for DC4 using dynamic responses excited at N2, N5, and N6

damage location, and this influence does not affect the performance of the method for damage detection and localization. However, it can be seen that different impact locations still result in slightly different  $DF_{FR}$ , which could be interpreted as better or worse results. This issue could be overcome by carrying out tests several times for different impact locations and analyzing the results comprehensively.

### 3.3 Analysis and result interpretations for the method using coefficients as $DF_{COEFF}$

In this section, the same sensor clustering-based ARX models are used to fit the acceleration data. However,  $DF_{COEFF}$  are applied using the square sum of the difference of the coefficients in ARX models as explained before. To distinguish the damaged state from the healthy state, the threshold is introduced which is still determined by comparing two healthy states. The  $DF_{COEFF}$  using the difference of coefficients are shown in Fig. 19. According to the observation, the threshold is set to 0.5 with 79 of the 80 points below it.

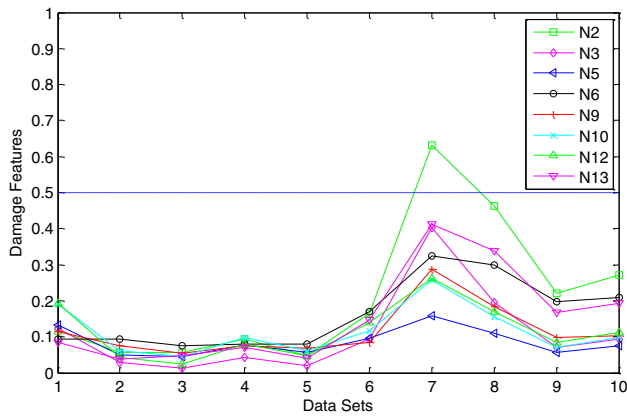


Fig. 19  $DF_{COEFF}$  for determining the threshold under free vibration

3.3.1 Damage detection using  $DF_{COEFF}$  for Damage Case 1 (DC1): scour (support removal) at N4

Since Damage Case 1 introduces a global damage caused by the removal of support at N4, the  $DF_{COEFF}$  for all the nodes are above the threshold (Fig. 20). Among them, the  $DF_{COEFF}$  for N3 and N4 are the highest, because they are closest to the damage. The indirect effect at N2 and N5 is also observed. For this case, the peak value of  $DF_{COEFF}$  is about 22, which will show that this damage is more severe than the change of boundary conditions in Damage Case 2 shown in the next section. Therefore, it is concluded that the method using  $DF_{COEFF}$  can simultaneously identify the location and estimate the severity for this case.

3.3.2 Damage detection using  $DF_{COEFF}$  for Damage Case 2 (DC2): boundary restraint (fixing the roller supports) at N7 and N14

Figure 21 plots the results for Damage Case 2. It is shown that the  $DF_{COEFF}$  for N6 and N13 are still higher than others because of fixing the roller supports at N7 and N14.

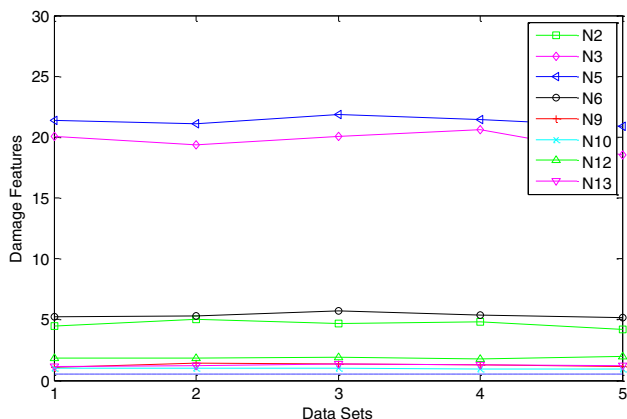


Fig. 20  $DF_{COEFF}$  for DC1 of the steel grid structure

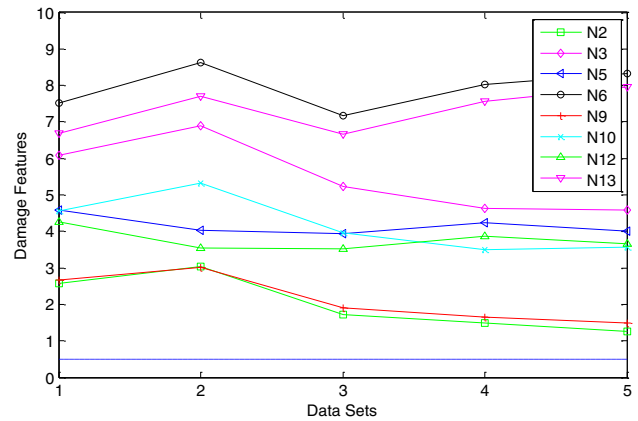


Fig. 21  $DF_{COEFF}$  for DC2 of the steel grid structure

The highest  $DF_{COEFF}$  shown in this case is 8.6. N2 and N9 have the lowest  $DF_{COEFF}$ , since they are farthest from the damage. However, N5 and N12 do not show higher  $DF_{COEFF}$  than N3 and N10 even though they are closer to the damage. Although the indirect effect is not identified, the direct influence of damage on N6 and N13 still reveals the location of damage successfully.

3.3.3 Damage detection using  $DF_{COEFF}$  for Damage Case 3 (DC3): moment release (removal of bolts) and plate removal at N3

Figure 22 shows the results for the localized damage due to the removal of plate and bolts simultaneously at N3 for Damage Case 3. As shown in the figure, only the  $DF_{COEFF}$  for N3 are clearly above the threshold, and all the other  $DF_{COEFF}$  are around or below the threshold, which accurately locates the damage. It is noted that the maximum  $DF_{COEFF}$  is 4.1, which is less than Damage Cases 1 and 2. This is consistent with the results for the  $DF_{FR}$  discussed in the previous sections.

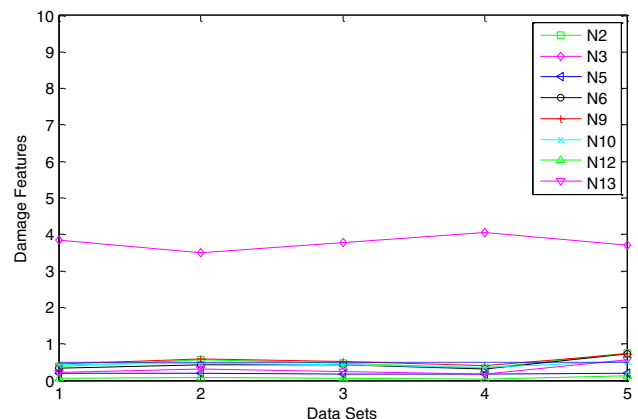
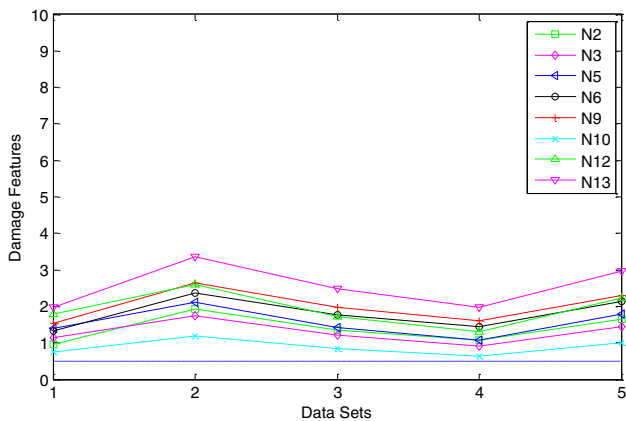


Fig. 22  $DF_{COEFF}$  for DC3 of the steel grid structure



**Fig. 23**  $DF_{COEFF}$  for DC4 of the steel grid structure

### 3.3.4 Damage detection using $DF_{COEFF}$ for Damage Case 4 (DC4): moment release (removal of bolts) at N3 and N10

Damage Case 4 is introduced by removing bolts at N3 and N10. The  $DF_{COEFF}$  for this case are shown in Fig. 23. It is seen that all the  $DF_{COEFF}$  are above the threshold based on the same reason as in Sect. 3.2.4. The maximum of  $DF_{COEFF}$  is 3.4 showing this damage is the least severe. However, the highest  $DF_{COEFF}$  is not for N3 or N10, which means that the damage is still not clearly located even if the coefficients are used as DFs.

## 4 Conclusions

In this paper, a new damage detection methodology is proposed by creating ARX models for different sensor clusters using the equations of motion of a structure. A unique advantage of the proposed method is that the order of the ARX models fixed, since it is directly derived from the EOM, offering opportunities for an easier automation and improved computational efficiency. Then, two different types of DFs derived from these models were introduced.  $DF_{FR}$  was based on the idea that the ARX models created for one state of the structure is no longer fit for another state.  $DF_{COEFF}$  related the change in coefficients to the change in stiffness. The proposed methodology is applied to experimental data obtained from a grid-type steel structure where different damage cases were simulated. Based on the results presented in the paper, it is concluded that both two kinds of DFs can identify and locate the damage in the steel grid structure and estimate the relative severity successfully, but  $DF_{FR}$  using fit ratios can provide more successful results for some cases. Although the results using  $DF_{COEFF}$  are not particularly superior to results obtained using  $DF_{FR}$  in the current form, this damage feature is still very important, since it may be

extensible to build a direct relationship between the change in coefficients and stiffness. However, there are still some limitations in these DFs. In this paper, it is shown that the DFs do not perform very well for combined damage and the damage that has more global effect. In the future, different combinations of coefficients and different statistical methods can be used to locate damage more accurately, or distinguish between the changes in mass and stiffness. Authors are also working on extending current research to ambient vibration data using some techniques, such as random decrement (RD) [42]. Another future research direction is to test the proposed method using experimental data from other laboratory and field structures.

**Acknowledgments** This research was supported by the Natural Sciences and Engineering Research Council of Canada through the Discovery Grants.

## References

- Little RG (2002) Controlling cascading failure: understanding the vulnerabilities of interconnected infrastructures. *J Urban Technol* 9(1):109–123
- Moore J, Glencross-Grant R, Mahini S, Patterson RA (2011) Towards predictability of bridge health. In: Proceedings of 2011 Regional Convention, pp 103–110
- Skulic J (2014) Wireless sensor networks using network coding for structural health monitoring. Dissertation, Imperial College London
- Federal Highway Administration (FHWA) (2011) Bridge Preservation Guide. US Department of Transportation, Washington, DC
- Federal Highway Administration (FHWA) (2015) Highway bridges by state and highway system 2015. <http://www.fhwa.dot.gov/bridge/nbi/no10/defbr15.cfm>. Accessed 9 Apr 2016
- Félio G (2012) Canadian Infrastructure Report Card, Vol. 1: Municipal Roads and Water Systems, Canadian Construction Association, Canadian Public Works Association, Canadian Society for Civil Engineering, Federation of Canadian Municipalities
- Mirza SM, Haider M (2003) The state of infrastructure in Canada: implications for infrastructure planning and policy. Infrastructure Canada
- Sohn H, Farrar CR, Hemez FM, Shunk DD, Stinemates DW, Nadler BR (2003) A review of structural health monitoring literature: 1996–2001, Report LA-13976-MS. Los Alamos National Laboratory, Los Alamos
- Bernal D, Beck J (2004) Preface to the special issue on phase I of the IASC-ASCE structural health monitoring benchmark. *J Eng Mech ASCE* 130(1):1–2
- Lynch JP, Loh KJ (2006) A summary review of wireless sensors and sensor networks for structural health monitoring. *Shock Vib Digest* 38(2):91–128
- Inaudi D, Glisic B (2008) Overview of 40 bridge monitoring projects using fiber optic sensors. In: Conference CD of the Fourth International Conference on Bridge Maintenance, Safety and Management (IABMAS '08), pp 2514–2521
- Fan W, Qiao P (2011) Vibration-based damage identification methods: a review and comparative study. *Struct Health Monit* 10(1):83–111

13. Malekzadeh M, Atia G, Catbas FN (2015) Performance-based structural health monitoring through an innovative hybrid data interpretation framework. *J Civil Struct Health Monit* 5(3):287–305
14. Li H, Ou J (2016) The state of the art in structural health monitoring of cable-stayed bridges. *J Civil Struct Health Monit* 6(1):1–25
15. Schallhorn C, Rahmatalla S (2015) Crack detection and health monitoring of highway steel-girder bridges. *Struct Health Monit* 14(3):281–299
16. Rytter A (1993) Vibration based inspection of civil engineering structures. Dissertation, Aalborg University
17. Jafarkhani R, Masri SF (2011) Finite element model updating using evolutionary strategy for damage detection. *Comput-Aided Civil Infrastruct Eng* 26(3):207–224
18. Siebel T, Friedmann A, Koch M, Mayer D (2012) Assessment of mode shape-based damage detection methods under real operational conditions. In: *Proceedings of the 6th European Workshop on Structural Health Monitoring (EWSHM)*, pp 130–137
19. An Y, Ou J (2013) Experimental and numerical studies on model updating method of damage severity identification utilizing four cost functions. *Struct Control Health Monit* 20(1):107–120
20. Hamze A, Gueguen P, Roux P, Baillet L (2014) Damage detection and localisation using mode-based method and perturbation theory. In: *Proceedings of the Seventh European Workshop on Structural Health Monitoring (EWSHM)*, pp 1728–1735
21. Sohn H, Farrar CR, Hunter NF, Worden K (2001) Structural health monitoring using statistical pattern recognition techniques. *J Dyn Syst Meas Contr* 123(4):706–711
22. Nair KK, Kiremidjian AS, Law KH (2006) Time series-based damage detection and localization algorithm with application to the ASCE benchmark structure. *J Sound Vib* 291(1):349–368
23. Gül M (2009) Investigation of damage detection methodologies for structural health monitoring. Dissertation, University of Central Florida
24. Magalhães F, Cunha A, Caetano E (2012) Vibration based structural health monitoring of an arch bridge: from automated OMA to damage detection. *Mech Syst Signal Process* 28:212–228
25. Kopsaftopoulos FP, Fassois SD (2013) A functional model based statistical time series method for vibration based damage detection, localization, and magnitude estimation. *Mech Syst Signal Process* 39(1):143–161
26. Andersen P (1997) Identification of civil engineering structures using ARMA models. Dissertation, Aalborg University
27. Bodeux JB, Golinvall JC (2000) ARMAV model technique for system identification and damage detection. In: *Proceedings of the European COST F3 Conference on System Identification and Structural Health Monitoring*, pp 303–312
28. Gül M, Catbas FN (2009) Statistical pattern recognition for structural health monitoring using time series modeling: theory and experimental verifications. *Mech Syst Signal Process* 23(7):2192–2204
29. Gül M, Catbas FN (2011) Structural health monitoring and damage assessment using a novel time series analysis methodology with sensor clustering. *J Sound Vib* 330(6):1196–1210
30. Van Le H, Nishio M (2015) Time-series analysis of GPS monitoring data from a long-span bridge considering the global deformation due to air temperature changes. *J Civil Struct Health Monit* 5(4):415–425
31. Yao R, Pakzad SN (2014) Damage and noise sensitivity evaluation of autoregressive features extracted from structure vibration. *Smart Mater Struct* 23(2):025007
32. Roy K, Bhattacharya B, Ray-Chaudhuri S (2015) ARX model-based damage sensitive features for structural damage localization using output-only measurements. *J Sound Vib* 349:99–122
33. Kim CW, Chang KC, Kitauchi S, McGetrick PJ (2016) A field experiment on a steel Gerber-truss bridge for damage detection utilizing vehicle-induced vibrations. *Structural Health Monitoring* 15(2):174–192
34. Ljung L (1999) *System identification: theory for the user*, 2nd edn. Prentice Hall, Upper Saddle River
35. Box GE, Jenkins GM, Reinsel GC (2013) *Time series analysis: forecasting and control*, 4th edn. Wiley, Hoboken
36. Levy H, Lessman F (1992) *Finite difference equations*. Dover Publications, Mineola
37. Catbas FN, Caicedo JM, Dyke SJ (2006) Development of a benchmark problem for bridge health monitoring. In: *Proceedings of the Third International Conference on Bridge Maintenance, Safety and Management (IABMAS)*, pp 16–19
38. Gül M, Catbas FN (2008) A new methodology for identification, localization and quantification of damage by using time series modeling. In: *Proceedings of the 26th International Modal Analysis Conference (IMAC XXVI)*, pp 4–7
39. Farrar CR, Lieven NA (2007) Damage prognosis: the future of structural health monitoring. *Philos Trans R Soc Lond A: Math, Phys Eng Sci* 365(1851):623–632
40. Farrar CR, Worden K (2012) *Structural health monitoring: a machine learning perspective*. Wiley, Hoboken
41. Dervilis N, Cross E, Barthorpe R, Worden K (2014) Robust methods of inclusive outlier analysis for structural health monitoring. *J Sound Vib* 333(20):5181–5195
42. Gül M, Catbas FN (2011) Damage assessment with ambient vibration data using a novel time series analysis methodology. *J Struct Eng* 137(12):1518–1526